J Mol Model (2013) 19:2149–2163
DOI 10.1007/s00894-012-1689-4

ORIGINAL PAPER

Conformational analysis of lignin models: a chemometric approach

Eduardo W. Castilho-Almeida · Wagner B. De Almeida · Hélio F. Dos Santos

Received: 30 May 2012 / Accepted: 12 November 2012 / Published online: 11 December 2012

Abstract In the present work, conformational analysis of lignin models was accomplished by considering four cross-link types (3–5′, β-5′, α-O-4 and β-O-4) and three monomer units [guaiacyl (G), p-hydroxyphenyl (H) and syringyl (S)]. Analysis involving the 3–5′ and β-5′ dimers was conducted following the standard procedure, i.e., rotating the monomers around the single bond. On the other hand, analysis of α-O-4 and β-O-4 dimers followed a distinct protocol with the aid of an interesting chemometric tool called Box-Behnken (BB) design. This methodology was applied with the aim of screening the most relevant dihedral angles. The results show that the conformational space for large systems with several dihedral angles can be mapped satisfactorily through the BB approach, reducing the number of dimensions to be treated at the quantum mechanical level. Furthermore, the quantum mechanics-chemometry-quantum mechanics (QM/BB/QM) method proposed here allows us to determine calculated torsional angles for lignin models in good agreement with crystallographic data for some model compounds.

Keywords Lignin · Box-Behnken design · Conformational analysis · Quantum mechanical calculation

Introduction

Plant cells have a special feature different from animal cells in that they exhibit great structural rigidity generated by a cell wall composed mainly of lignin—the second most abundant polymeric material on Earth [1–14]. All vegetal materials have a large amount of this polymer (about 25 % in mass on vegetal biomass [12]) occurring together with cellulose and hemicellulose—the main macromolecules in plant-based biomass. Unlike cellulose, which has only one monomeric unit in its polymeric structure, lignin has no well-defined structure. Its structure comprises distinct phenolic units, mainly coniferyl [Guiacyl (G)], *para*-cumaryl [*p*-hydroxyphenyl (H)] and synapyl [syringyl (S)] alcohols. In addition, the structural complexity of this material is increased by the several link possibilities allowed between monomer units, namely inter-monomer cross-links, which are verified in different proportions depending on each vegetal species (Fig. 1).

The experimental literature reports the massive presence of four main kinds of cross-links between the phenolic units (β-O-4, α-O-4, β-5′ e 3–5′) that comprise about 80 % of native lignin (Table 1) [12, 14, 15]. Within this scenario we note that lignin has a notably complex structure and, therefore, the proposal of a representative molecular model for lignin structure is a difficult and challenging task involving several variables. This fact is reflected in the number of molecular modeling papers appearing in the literature that seek a representative model for natural polymers [2, 5, 7, 13, 16–26]. Among them, we highlight those focusing on the theoretical study of possible cross-links between the monomeric units of lignin [2, 5, 22, 23, 25]. The use of lower molecular weight models constitutes an interesting approach to clarify the subtle differences between cross-links involving similar structures of the phenolic units (G, S or H) [16]. Furthermore, the study of small models can also help evaluate, at a molecular level, the potential applicability of lignin in recovery processes, due to its abundant availability as a by-product [12]. Moreover, the use of template molecules is partially justified by experimentalists, who have demonstrated that, after a pre-treatment process, lignin chains are found in a fragmented form. This outcome was

E. W. Castilho-Almeida (✉) · H. F. Dos Santos
Departamento de Química, ICE,
Universidade Federal de Juiz de Fora, Campus Universitário,
36036-330 Juiz de Fora, MG, Brazil
e-mail: eduwalneide@uol.com.br

W. B. De Almeida
Departamento de Química, ICEx,
Universidade Federal de Minas Gerais, Campus Universitário,
31270-901 Belo Horizonte, MG, Brazil

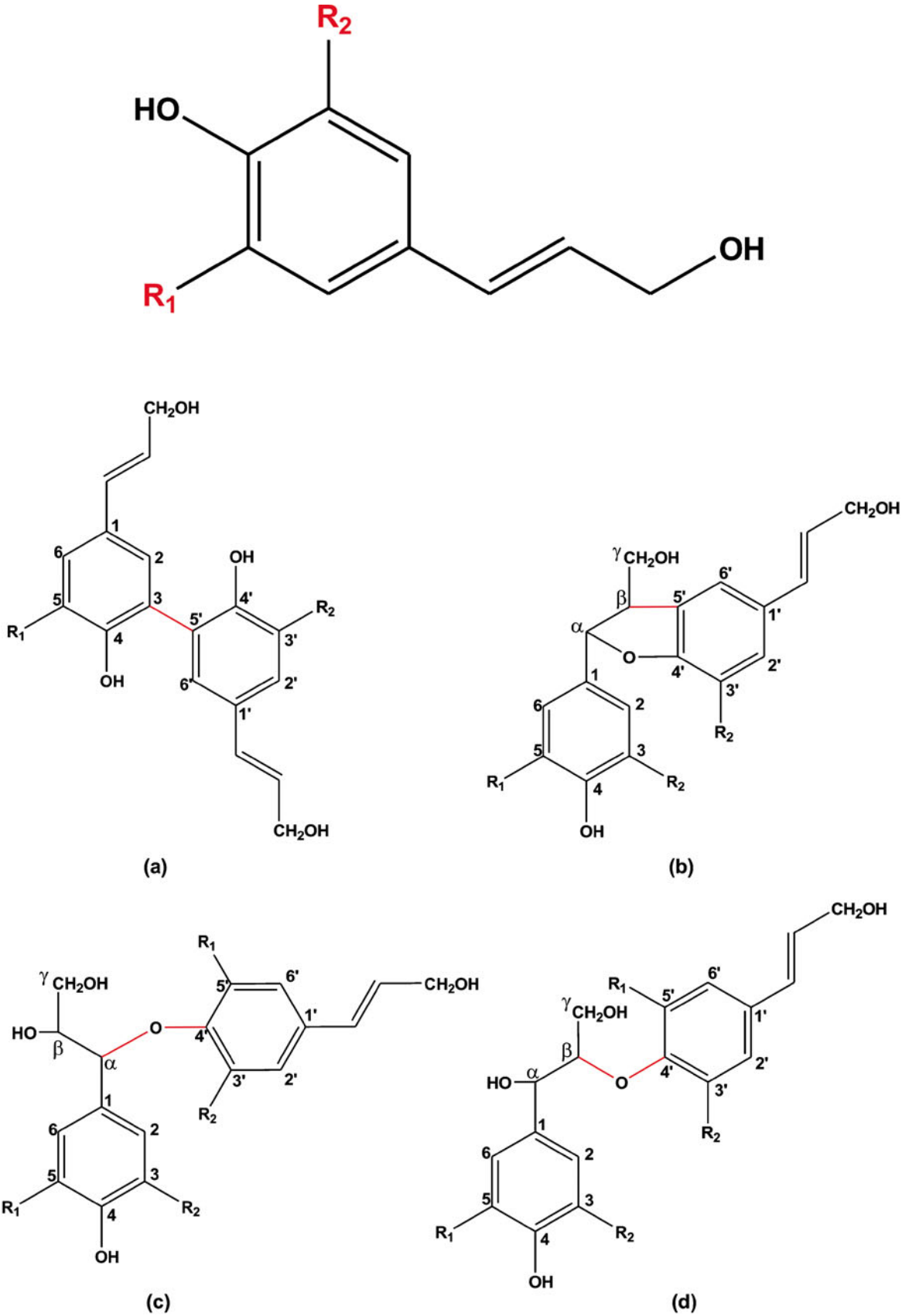

Fig. 1a–d General structure of a lignin monomer and the main cross-links found between monomers. **a** 3–5′, **b** β–5′, **c** α–O–4, **d** β–O–4. In the general structure $R_1 = R_2 = H$ (*p*-hydroxyphenyl, *H*); $R_1 = OCH_3$ and $R_2 = H$ (guaiacyl, *G*); $R_1 = R_2 = OCH_3$ (syringyl, *S*)

Table 1 The main cross-links between phenolic monomers found in native lignin

Cross-link[a]	Relative abundance (%)
β-O-4	48
β-5′	9–12
α-O-4	6–8
3–5′	9.5–11

[a]The basic structures are represented in Fig. 1

explored recently by Kim and coworkers [14], who obtained dissociation energy values for different cross-links found in lignin using small molecular models. The aim of that study was, according to the authors, to elucidate the mechanistic possibilities for lignin degradation by thermal or catalytic action.

In the present work, lignin dimers were submitted to a conformational analysis using a chemometric tool previously used by us [27] called Box-Behnken (BB) design. This statistical tool enables a concomitant conformational analysis of several dihedrals angles in lignin systems, accounting for individual and coupled effects of the set of angles. Figure 2 clearly shows the four main experimentally verified cross-links that are studied in this work.

Methods

The 24 dimers illustrated in Table 2 were studied in the present work. They were built considering the three monomeric units (G, H and S) cross-linked in pairs (considering the four main cross-link types—Table 1). Some previous studies in the literature have described some conformational analysis methods applied to small lignin models. The torsion angles that were selected for conformational analysis are dependent on the cross-link type. For structures containing β–5′ and 3–5′ cross-links, only one important torsional angle was selected; whereas for those structures containing α–O–4 and β–O–4 cross-links type, four dihedral angles are relevant to map the conformational space (see Fig. 3). All 24 geometries were optimized in gas phase at the HF/6-31G level and the final structures were used as initial guesses for conformational analysis.

For the models β–5′ and 3–5′, the conformational search for 12 dimers (β–5′–GG, GH, GS, HH, HS, SS and 3–5′–GG, GH, GS, HH, HS, SS) was performed directly through rotation around the inter-monomers bond, using 36 steps of 10° using the SCAN keyword in Gaussian 03 package at HF/6-31G level and keeping the geometry frozen (rigid-rotor approach) [28]. As a statistical-based method was used, no topological parameters other than the selected dihedral angles should vary. Therefore, the rigid SCAN excludes the influence of other variables on the description of conformational energy.

For the other two models (α–O–4–GG, GH, GS, HH, HS, SS and β–O–4–GG, GH, GS, HH, HS, SS) a different protocol for the conformational search, based on chemometry with the aid of BB design, was used [29]. This strategy was applied to systems with four relevant dihedrals, taking into consideration the weight of the interaction between them (see [18] for details). In this first analysis, we considered only the torsional angles directly involved in the cross-linking moiety, which were based on those used by Besombes and coworkers [23]. In other words, the BB design allows us to screen through the four main dihedral angles and find out the two most relevant, which are used further for potential energy surface (PES) calculation using a quantum mechanical (QM) method. As the first step in the BB analysis, the three levels of the variables (dihedral angles) were defined, namely low (−1), medium (0) and high (+1), which will define the response's matrix (total energies). This was done by taking the optimized geometry as low level (−1) and the geometries twisted by 45° and 90° as medium (0) and high (+1) levels, respectively. The dihedral angles used as input for BB analysis are given in Table 3.

Based on the energy values obtained for the sampling of 81 conformers (3^4 that means four dihedral angles at three levels) only 25 conformers were selected according to BB methodology. The number of conformers considered (N) is defined according to Equation 1, where k is the number of variables to be evaluated and C_0 is the number of central points (i.e., attempts considering the level 0 for all variables) [29]. As BB design is an incomplete factorial design, screening over variables is made by considering several 2^2 factorial analysis (two variables at two levels) maintaining the other two variables at the medium level (0). This process is performed six times, covering all possible combinations among the variables. Using the information provided by BB design we can set up the equation for the predictive model (Equation 2) where the β_i parameters are obtained from Equation 3.

$$N = 2k(k-1) + C_0 \tag{1}$$

$$\hat{y} = \hat{\beta}_0 + \sum_{i=1}^{k} \hat{\beta}_i \omega_i + \sum_{i=1}^{k} \hat{\beta}_{ii} \omega_i^2 + \sum_i \sum_j \hat{\beta}_{ij} \omega_i \omega_j + r_i \tag{2}$$

$$\beta = \left(X^T \cdot X\right)^{-1} \cdot \left(X^T \cdot Y\right) \tag{3}$$

In Equation 2, each β_i corresponds to the adjusted coefficient related to the ω_i parameter (torsional angle). The β_{ii} terms refer to the square combination of the ω_i angle responsible for the curvature associated to the quadratic model, and the β_{ij} terms are the crossed terms associated directly to interaction effects among the ω_i variables. The calculation of these parameters (Equation 3) takes into consideration the planning matrix (**X**—considering the codified variables) and

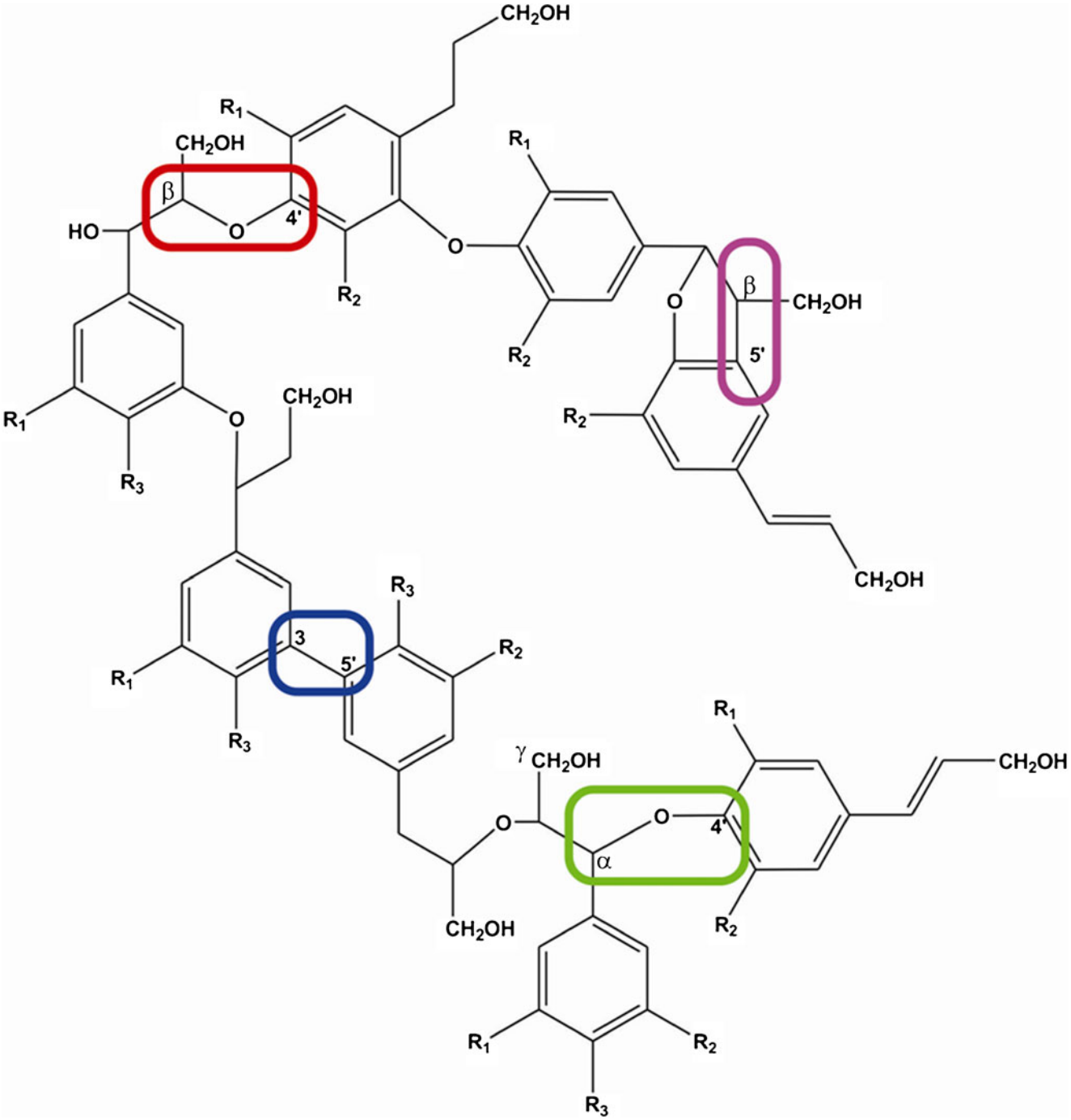

Fig. 2 Lignin model highlighting the four main cross-links between phenolic units

the response matrix (**Y**—total energy values for 25 conformers). To validate the predictive model, two important statistical parameters were evaluated: the Shapiro-Wilk (SW), to verify the normal distribution of residues (the difference between the observed and calculated energies for each conformer); and the graphs for normal distribution of effects that allows understanding of the weight of each effect to the responses. Following analysis of the predictive models, the two main dihedral angles were selected and used for construction of QM PES at the HF/6-31G level. This was done in a similar way as for the simpler dimers, using 10 steps of 36° for each dihedral. From the PES, those structures that were energetically more stable were selected and analyzed at different levels of theory, namely HF/6-31 + G(2d), B3LYP/6-31G and B3LYP/6-31 + G(2d), in order to assess the role of level of theory to the conformational distribution.

Table 2 Optimized geometries (HF/6-31G) of lignin dimers studied here

	Cross-link*			
	α-O-4	β-O-4	β-5’	3-5’
GG	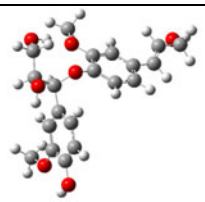	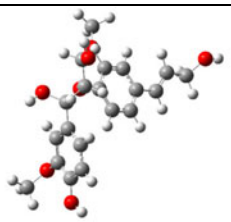	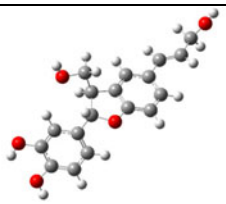	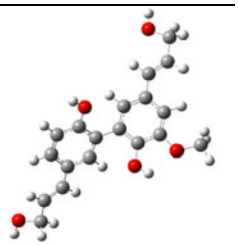
GH	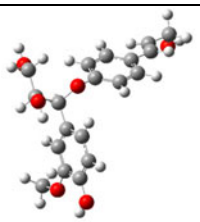	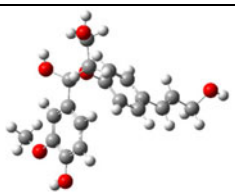	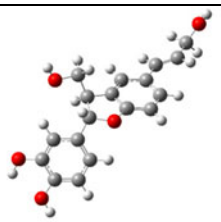	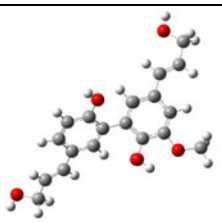
GS	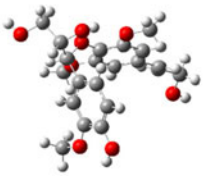	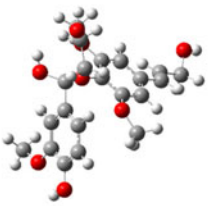	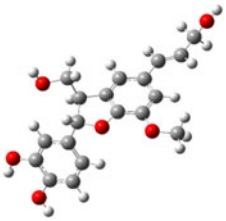	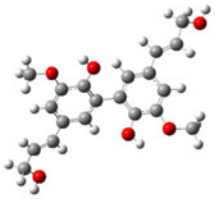
HH	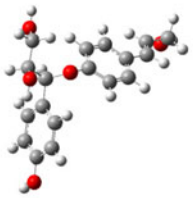	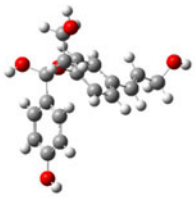	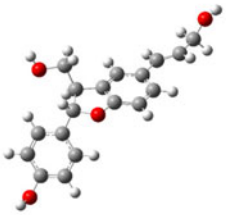	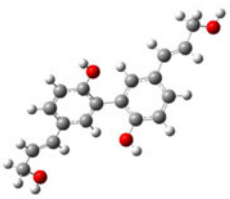
HS	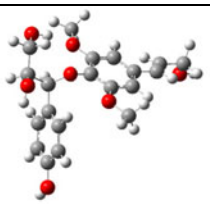	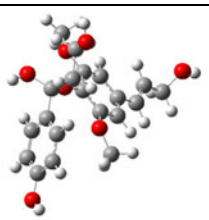	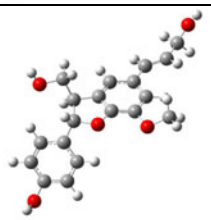	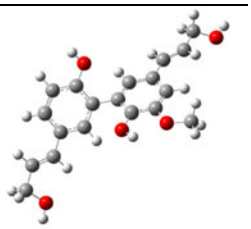
SS	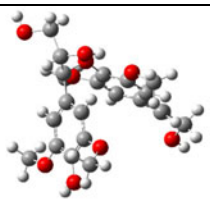	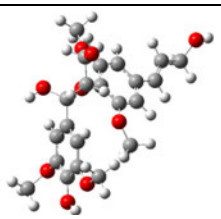	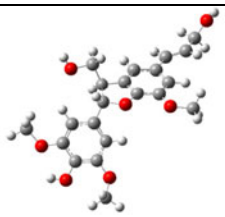	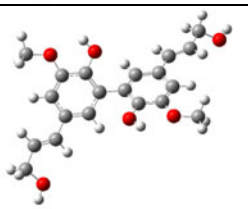

* See Fig. 1

Results and discussion

3–5′ and β–5′ dimers

The 3–5′ e β-5′ lignin models have only one important dihedral angle for conformational analysis (Fig. 3a,b). The stepwise potential energy curve (PEC) is represented in Fig. 4a,b (3–5′ and β–5′). From Fig. 4, it is clear that the PEC profiles depend only on the type of cross-link. However, small differences could be verified for different monomer combinations mainly at the barriers. These are related to the different R radicals on each monomer type. For the 3–5′

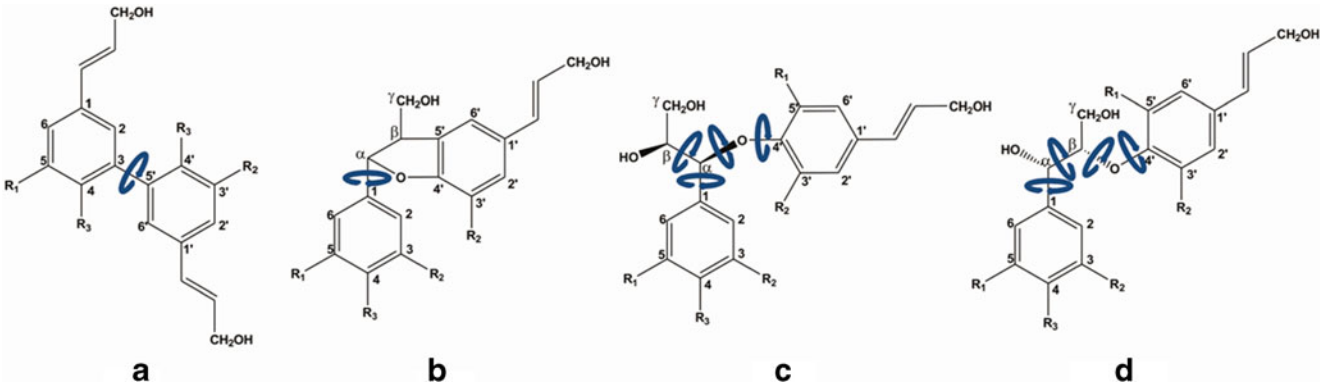

Fig. 3a–d General structures of lignin dimers showing the evaluated dihedral angles in the conformational analysis procedure. **a** 3–5′: $\omega_{1[3-5']}$(C2,C3,C5′,C6′); **b** β–5′: $\omega_{1[\beta-5]}$(C6,C1,Cα,O); **c** α–O–4: $\omega_{1[\alpha-O-4]}$(C2,C1,Cα,Cβ), $\omega_{2[\alpha-O-4]}$(Cγ,Cβ,Cα,O), $\omega_{3[\alpha-O-4]}$(Cβ,Cα,O,C4′) and $\omega_{4[\alpha-O-4]}$(Cα,O,C4′,C5′), **d** β–O–4: $\omega_{1[\beta-O-4]}$(C2,C1,Cα,Cβ), $\omega_{2[\beta-O-4]}$(C1,Cα,Cβ,Cγ), $\omega_{3[\beta-O-4]}$(Cγ,Cβ,O,C4′) and $\omega_{4[\beta-O-4]}$(Cβ,O,C4′,C3′). The α-O-4 (*erythro* αS, βS), β-O-4 (*erythro* αS, βS) and *trans* β-5′ model compounds were considered in the present work

dimers, two minima were found. The first, at around 65°, is separated from the second minimum (global minimum at ω= 126–129°; Table 4) by a small barrier around 90°. These values are in agreement with X-ray data for a similar lignin model involving the 3–5′ cross-link between aromatic rings (~65° and ~121° [30]). The rotation barrier is much lower than that found close to 180°, which is in accordance to some theoretical data obtained at the same theory level for a similar model [31]. These barriers noted on PEC are due to planar structures that favor π-conjugation between aromatic rings, besides increase the steric repulsion between the groups linked in the ortho-position. The planar structures correspond to transition state (TS) structures higher in energy by 0.5–1.0 kcalmol^{-1} (90°) and 10–14 kcalmol^{-1} (180°) than the minimum points. The TS structures were not further optimized.

For the β-5′-type dimers (Fig. 4b) two distinct minima points were noted around 0° (360°) and 180°. The very small energy differences found here are related to the asymmetry of monomers because of different R groups linked in aromatic units. Between both regions we observe two potential energy barriers at 60° and 240° where repulsion between phenolic hydrogens at C2 and C6 and the hydrogen linked at Cβ in the same monomeric unit is pronounced. Furthermore, the two inflections around 115° and 305° can be explained by the repulsion verified between the phenolic hydrogen at C2 and C6 and the hydrogen linked at Cα (slightly further away from C2/C6 hydrogen than Cβ hydrogen). The dihedral angle for the global minimum after geometry optimization was in the range of 175–179° (Table 4). This value is larger than the experimental data (144°) [32], due mainly to the lack of intermolecular interactions in the calculations.

α-O-4 and β-O-4 models

The PES for the previously lignin dimers (3–5′ and β–5′) are notably simple. However, for the α–O–4 and β–O–4-type dimers four important torsional angles must be included in the conformational searching. For flexible molecules, random methods such as Monte Carlo are usually preferable over systematic approaches. Here, we propose a distinct protocol based on a sequential approach including quantum mechanics-chemometry-quantum mechanics (QM/BB/QM). First the QM method is used to generate the input data, which are treated by chemometric tools, reducing the number of variable (dihedral angles) to be further included in the QM analysis. The torsional angles shown in Fig. 3c,d were considered. Their initial values were obtained from the optimized structures at the HF/6-31G level of theory and labeled as low level (−1) in the BB 3^4 protocol. The other two levels were determined by adding 45° to the initial value to obtain the medium level (0) and further 45° to achieve the high level (+1). A total of 25 different protocols were implemented for each dimer.

Following our sequential protocol, the first step was implemented to calculate the energy of all 81 forms possible (3x3x3x3) at the HF/6-31G level of theory. From these structures, 25 conformers were evaluated according to the BB 3^4 planning matrix (**X** matrix) and their respective total energies used as response (**Y** matrix). In principle, the analysis of these 25 attempts allows us to establish an equation that accounts for effects of the four dihedral angles on the total energy. In the present work, a complete quadratic model was fitted as generically presented by Equation 2. The adjusted equations that describe the molecular energy as a function of ω_i are shown in Table 5. For the SW test, a calculated value larger than the reference ($SW_{calc} > SW_{ref(25;5\ \%)} = 0.918$) answers the expectations for a normal distribution of residues. It allows some statistical inferences, which evidence the suitability of the predictive models. All 12 models evaluated have presented statistical signs of normal distribution of residues (i.e., $SW_{calc} > SW_{ref}$).

The next step in the sequential protocol was to determine the two main dihedral angles playing a major role in conformational stability. This was done based on analysis of the

Table 3 Values of dihedral angles according to the Box-Behnken (BB) design levels

Dihedral	Cross-link	Dimer	Level		
			−1	0	+1
ω_1	α-O-4 (C2,C1,Cα,Cβ)	GG	102.5	147.5	192.5
		GH	91.8	136.8	181.8
		GS	143.5	188.5	233.5
		HH	93.4[a]	133.4[a]	173.4[a]
		HS	99.6	144.6	189.6
		SS	141.3[a]	176.3[a]	211.3[a]
	β-O-4 (C2,C1,Cα,Cβ)	GG	−81.2	−36.2	8.9
		GH	−85.3	−40.3	4.7
		GS	−81.8	−36.8	8.2
		HH	−79.4	−34.4	10.6
		HS	−76.4	−31.4	13.6
		SS	−77.8	−32.8	12.2
ω_2	α-O-4 (Cγ,Cβ,Cα,O)	GG	47.4	92.4	137.4
		GH	54.0	99.0	144.0
		GS	70.6	115.6	160.6
		HH	52.9[a]	92.9[a]	132.9[a]
		HS	46.5	91.5	136.5
		SS	70.8[a]	105.8[a]	140.8[a]
	β-O-4 (C1,Cα,Cβ,Cγ)	GG	179.6	224.6	269.6
		GH	168.9	213.9	258.9
		GS	167.6	212.6	257.6
		HH	178.3	223.3	268.3
		HS	177.8	222.8	267.8
		SS	−179.9	−134.9	−89.9
ω_3	α-O-4 (Cβ,Cα,O,C4′)	GG	−162.6	−117.6	−72.6
		GH	−146.5	−101.5	−56.5
		GS	148.8	193.8	238.8
		HH	−146.7[a]	−106.7[a]	−66.7[a]
		HS	−163.1	−118.1	−73.1
		SS	148.4[a]	183.4[a]	218.4[a]
	β-O-4 (Cγ,Cβ,O,C4′)	GG	93.7	138.7	183.7
		GH	111.8	156.8	201.8
		GS	84.0	129.0	174.0
		HH	99.2	144.2	189.2
		HS	81.1	126.1	171.1
		SS	81.1	126.1	171.1
ω_4	α-O-4 (Cα,O,C4′,C5′)	GG	−108.6	−63.6	−18.6
		GH	−123.0	−78.0	−33.0
		GS	−106.5	−61.5	−16.5
		HH	−123.6[a]	−83.6[a]	−43.6[a]
		HS	−115.5	−70.5	−25.5
		SS	−104.2[a]	−69.2[a]	−34.2[a]
	β-O-4 (Cβ,O,C4′,C3′)	GG	−100.7	−55.7	−10.7
		GH	−133.7	−88.7	−43.7
		GS	−108.9	−63.9	−18.9
		HH	−127.7	−82.7	−37.7
		HS	−110.4	−65.4	−20.4
		SS	−109.9	−64.9	−19.9

[a]Dimers twisted by different values (not 45° per level) due to steric hindrance

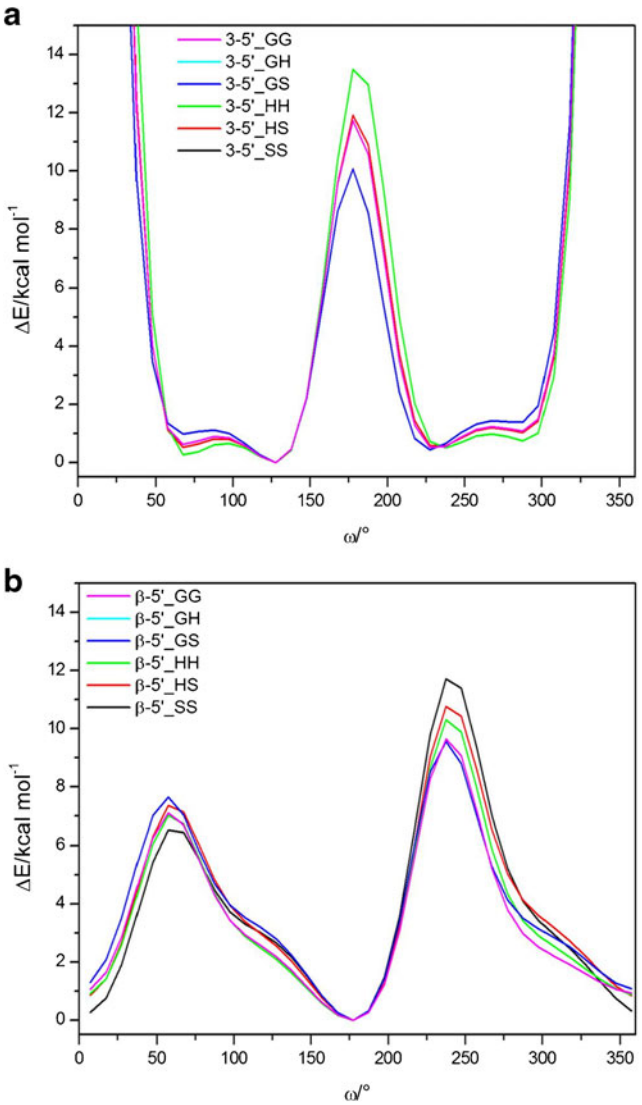

Fig. 4 HF/6-31G potential energy curve (PEC) obtained from conformational analysis of **a** 3–5′ and **b** β-5′-type dimers considering the different phenolic units G, H and S

graph of the normal distribution of effects (NDE), which is a plot of the normal standard distribution z ≈ N(0,1) (vertical axis) against the effects (horizontal axis). These effect values are obtained as twice the estimated values (the coefficients of the fitted model—β—presented in Eqs. 2 and 3). It can be understood from the algorithm used to calculate the estimators' model that the true values of factors levels were substituted by 0,− 1 and +1 due to the codifications of the original variables. This codification, i.e., the statistical model, consists mathematically of setting the axis origin at an intermediate value. In the present case the origin axis is the half the amplitude of the corresponding factor variation. For this reason, to cover whole sampling area, the effects are in fact double the estimators' model. The NDE graphs for the α-O-4 and β-O-4 dimer are plotted in Fig. 5. Those points that are correlated linearly correspond to random effects, and are not representative of the adjusted model. On the other hand, points that do not follow the linear behavior are significant to the energy description, the significance becoming higher the more distant from the linear region the point is. As verified, of the six α-O-4-type dimers studied, five have $\omega_{2[\alpha\text{-O-4}]}$(Cγ, Cβ, Cα, O) and $\omega_{3[\alpha\text{-O-4}]}$(Cβ, Cα, O, C4′) as the main dihedral angles, highlighting the importance of such dihedral angles for structural stability. These angles define the conformation of the side chain linked to the aromatic rings and the connection between the aromatic units, respectively. A similar analysis was carried out for β-O-4 dimers. Of the six molecules studied, five showed the $\omega_{3[\beta\text{-O-4}]}$(Cγ, Cβ, O, C4′) as the most significant torsional angle, and four also showed $\omega_{1[\beta\text{-O-4}]}$(C2, C1, Cα, Cβ) as an important torsional angle for conformational analysis. The reason to $\omega_{3[\beta\text{-O-4}]}$ appears as a relevant dihedral angle is based on the proximity of the Cγ hydroxyl and R groups linked at the neighboring phenolic unit. This proximity might facilitate the hydrogen bond between these two groups, influencing greatly the calculated energy. The relevance of the $\omega_{1[\beta\text{-O-4}]}$ dihedral is related to the proximity of the phenolic hydrogen at C2 and C6 and the Cα hydroxyl, leading to the same situation as in the previous case. Furthermore, it is worth noting that some interaction effects between dihedral angles have great significance. For example, the $\omega_1.\omega_3$ interaction in the α-O-4_SS dimer (Fig. 5f) shows a particular significance in the total energy. These dihedrals angles—$\omega_{1[\alpha\text{-O-4}]}$(C2, C1, Cα, Cβ) and $\omega_{3[\alpha\text{-O-4}]}$(Cβ, Cα, O, C4′)—are consecutive on the molecule; therefore they interact and can influence the conformational energy directly if one of them presents a high effect. This is a particular feature of the BB design that provides important information about crossed-effects between variables. Thus, in short, from the BB analysis, two dihedral angles were selected for each type of dimer. These outcomes make feasible the systematic conformational analysis through QM methods as described in the next paragraphs as the final part of our protocol.

The selected pairs of torsional angles for each dimer were rotated ten times in steps of 36°, generating 121 conformers.

Table 4 Dihedral angle values for the lowest energy conformers obtained from the PEC for 3–5′ and β-5′ at HF/6-31G level of theory

		Dimers					
		GG	GH	GS	HH	HS	SS
Cross-link	3–5′	127.8°	127.8°	129.2°	126.0°	127.4°	129.2°
	β–5′	177.4°	177.4°	178.7°	176.4°	176.4°	175.8°

Table 5 BB-adjusted equations representing the total energy as a function of the dihedral angles

		Adjusted model equation according to BB model[a]	SW	Main dihedrals
α-O-4	GG	$-1294 + 0.07\omega_1 + 1.16\omega_2 + 0.08\omega_3 - 0.05\omega_4 - 0.15\omega_1.\omega_2 - 0.42\omega_1.\omega_3 - 0.09\omega_1.\omega_4 c$	0.966	ω_2 (Cγ,Cβ,Cα,O)
		$-0.17\omega_2.\omega_3 + 0.11\omega_2.\omega_4 - 0.02\omega_3.\omega_4 + 0.16{\omega_1}^2 + 0.91{\omega_2}^2 + 0.37{\omega_3}^2 - 0.12{\omega_4}^2$		ω_3 (Cβ,Cα,O,C4′)
	GH	$-1180 + 0.26\omega_1 + 1.30\omega_2 - 0.08\omega_3 - 0.07\omega_4 - 0.31\omega_1.\omega_2 - 0.08\omega_1.\omega_3 - 0.10\omega_1.\omega_4$	0.977	ω_2 (Cγ,Cβ,Cα,O)
		$+0.05\omega_2.\omega_3 + 0.12\omega_2.\omega_4 - 0.01\omega_3.\omega_4 + 0.08{\omega_1}^2 + 1.10{\omega_2}^2 + 0.23{\omega_3}^2 - 0.05{\omega_4}^2$		ω_1 (C2,C1,Cα,Cβ)
	GS	$-1393 + 6.36\omega_1 + 3.56\omega_2 - 7.01\omega_3 - 0.66\omega_4 + 0.82\omega_1.\omega_2 - 15.4\omega_1.\omega_3 - 1.40\omega_1.\omega_4$	0.918	ω_1 (C2,C1,Cα,Cβ)
		$-0.83\omega_2.\omega_3 + 0.07\omega_2.\omega_4 - 1.80\omega_3.\omega_4 + 0.63{\omega_1}^2 - 6.25{\omega_2}^2 - 1.76{\omega_3}^2 - 9.75{\omega_4}^2$		ω_3 (Cβ,Cα,O,C4′)
	HH	$-1066 - 0.06\omega_1 + 0.64\omega_2 + 0.17\omega_3 - 0.06\omega_4 - 0.22\omega_1.\omega_2 - 0.02\omega_1.\omega_3 - 0.08\omega_1.\omega_4$	0.954	ω_2 (Cγ,Cβ,Cα,O)
		$-0.01\omega_2.\omega_3 + 0.09\omega_2.\omega_4 - 0.01\omega_3.\omega_4 + 0.05{\omega_1}^2 + 0.50{\omega_2}^2 + 0.11{\omega_3}^2 - 0.01{\omega_4}^2$		ω_3 (Cβ,Cα,O,C4′)
	HS	$-1294 + 0.56\omega_1 + 1.36\omega_2 - 0.63\omega_3 - 0.03\omega_4 - 0.02\omega_1.\omega_2 - 1.71\omega_1.\omega_3 - 0.10.\omega_1.\omega_4$	0.941	ω_2 (Cγ,Cβ,Cα,O)
		$-0.77.\omega_2.\omega_3 + 0.08\omega_2.\omega_4 - 0.12\omega_3.\omega_4 + 0.55{\omega_1}^2 + 0.87{\omega_2}^2 + 1.06{\omega_3}^2 - 0.42{\omega_4}^2$		ω_3 (Cβ,Cα,O,C4′)
	SS	$-1514 + 0.33\omega_1 + 3.39\omega_2 - 1.17\omega_3 + 0.76\omega_4 + 0.85\omega_1.\omega_2 + 2.69\omega_1.\omega_3 + 0.39\omega_1.\omega_4$	0.948	ω_2 (Cγ,Cβ,Cα,O)
		$+0.11\omega_2.\omega_3 - 1.91\omega_2.\omega_4 - 1.37\omega_3.\omega_4 - 2.06{\omega_1}^2 - 0.85{\omega_2}^2 - 2.99{\omega_3}^2 - 3.61{\omega_4}^2$		ω_3 (Cβ,Cα,O,C4′)
β-O-4	GG	$-1294 + 1.38\omega_1 - 0.29\omega_2 + 1.11\omega_3 + 0.24\omega_4 - 0.02\omega_1.\omega_2 + 0.07\omega_1.\omega_3 - 0.06\omega_1.\omega_4$	0.969	ω_1 (C2,C1,Cα,Cβ)
		$-0.81\omega_2.\omega_3 + 0.67\omega_2.\omega_4 + 1.46\omega_3.\omega_4 + 0.49{\omega_1}^2 + 0.22{\omega_2}^2 + 0.85{\omega_3}^2 + 0.60{\omega_4}^2$		ω_3 (Cγ,Cβ,O,C4′)
	GH	$-1180 + 0.24\omega_1 - 1.30\omega_2 + 0.54\omega_3 + 0.86\omega_4 - 0.62\omega_1.\omega_2 - 0.01\omega_1.\omega_3 + 0.10\omega_1.\omega_4$	0.943	ω_2 (Cβ,O,C4′,C3′)
		$-1.35\omega_2.\omega_3 - 2.45\omega_2.\omega_4 + 0.25\omega_3.\omega_4 - 0.64{\omega_1}^2 + 1.73{\omega_2}^2 - 0.09{\omega_3}^2 + 0.86{\omega_4}^2$		ω_4 (C1,Cα,Cβ,Cγ)
	GS	$-1408 + 0.02\omega_1 - 0.29\omega_2 + 0.76\omega_3 - 0.86.\omega_4 + 0.41\omega_1.\omega_2 + 0.01\omega_1.\omega_3 - 0.18\omega_1.\omega_4$	0.918	ω_3 (Cγ,Cβ,O,C4′)
		$+1.09\omega_2.\omega_3 + 0.95\omega_2.\omega_4 - 1.82\omega_3.\omega_4 - 0.51{\omega_1}^2 - 0.42{\omega_2}^2 + 0.91{\omega_3}^2 + 1.10{\omega_4}^2$		ω_4 (C1,Cα,Cβ,Cγ)
	HH	$-1066 + 1.40\omega_1 - 0.10\omega_2 + 0.45\omega_3 - 0.29\omega_4 + 0.01\omega_1.\omega_2 + 0.07\omega_1.\omega_3 - 0.05\omega_1.\omega_4$	0.947	ω_1 (C2,C1,Cα,Cβ)
		$-0.19\omega_2.\omega_3 + 0.66\omega_2.\omega_4 - 0.02\omega_3.\omega_4 + 0.86{\omega_1}^2 + 0.25{\omega_2}^2 + 0.16{\omega_3}^2 + 0.26{\omega_4}^2$		ω_3 (Cγ,Cβ,O,C4′)
	HS	$-1294 + 1.27\omega_1 - 0.44\omega_2 + 0.55\omega_3 - 0.18\omega_4 + 0.01\omega_1.\omega_2 + 0.05\omega_1.\omega_3 + 0.05\omega_1.\omega_4$	0.932	ω_1 (C2,C1,Cα,Cβ)
		$-0.12\omega_2.\omega_3 + 0.61\omega_2.\omega_4 + 0.35\omega_3.\omega_4 + 0.76{\omega_1}^2 + 0.13{\omega_2}^2 + 0.30{\omega_3}^2 + 0.45{\omega_4}^2$		ω_3 (Cγ,Cβ,O,C4′)
	SS	$-1522 + 1.27\omega_1 - 0.07\omega_2 + 0.61\omega_3 - 0.15\omega_4 + 0.01\omega_1.\omega_2 + 0.05\omega_1.\omega_3 + 0.02\omega_1.\omega_4$	0.944	ω_1 (C2,C1,Cα,Cβ)
		$-0.17\omega_2.\omega_3 + 0.60\omega_2.\omega_4 + 0.38\omega_3.\omega_4 + 0.70{\omega_1}^2 + 0.14{\omega_2}^2 + 0.37{\omega_3}^2 + 0.47{\omega_4}^2$		ω_3 (Cγ,Cβ,O,C4′)

[a] Values for ω_1, ω_2, ω_3 and ω_4 can range between $\{\omega_i \in \mathbb{R} \mid \omega_i \in [-1,1]\}$

Among the four dihedrals considered, the two least significant were kept fixed at their optimized values during this procedure. The PES created for all 12 structures examined are depicted in Fig. 6. From the analysis of individual PES, the five lowest energy minima points (S1, S2, S3, S4 and S5) were selected for each dimer. These selected structures were then optimized at the HF/6-31G theory level to guarantee full convergence of geometry. Table 6 shows the two main dihedral angles optimized for the five conformers (S1, S2, S3, S4 and S5) studied. The initial geometries, which correspond to the level (−1,−1, −1,−1), are labeled as S1. As noted in Table 6, most of the selected minima (S2–S5) differ from the initial point, and generally lead to conformers with lower energies than those originally proposed. This fact validates the sequential protocol used here as a conformational search approach able to find out the most stable structures, regardless of the reference set used. The relative energy for the distinct conformers, within the same class of dimer, was not higher than 10 kcalmol^{-1}, with the average being around 4 kcalmol^{-1} (Table 7).

Aiming to assess the role of level of theory on our conformational analysis, the lowest energy structures (noted in Tables 6 and 7) were optimized at the HF/6-31 + G(2d), B3LYP/6-31G and B3LYP/6-31 + G(2d) levels of theory—labeled as L2, L3 and L4 levels, respectively (see Table 6). The levels of theory used here usually do not change the conformations significantly. Some deviations noted for α-O-4_GH dimer are due to free rotation of the aromatic ring around the single bond allowing two stable points found about 180° apart from each other. As observed in Table 6, the basis set plays a major role in determining the geometry. The L2 and L4 levels [both considering 6–31 + G(2d)] show dihedral values generally closer to the predicted BB value for a minimum energy structures (BB values were obtained from Eq. 4 and Table 5). Comparison between some torsional angles from β-O-4_HH and β-O-4_SS models with experimental and theoretical data from the literature also reveals the primary role of the basis set for geometry as seen in Table 8. Furthermore, analysis of torsional angles allows us to validate the BB methodology used in this study once the topological parameters converge to crystallographic structure and theoretical values using well-established methodologies.

$$\frac{\partial E}{\partial \omega_1} = \frac{\partial E}{\partial \omega_2} = \frac{\partial E}{\partial \omega_3} = \frac{\partial E}{\partial \omega_4} = 0 \tag{4}$$

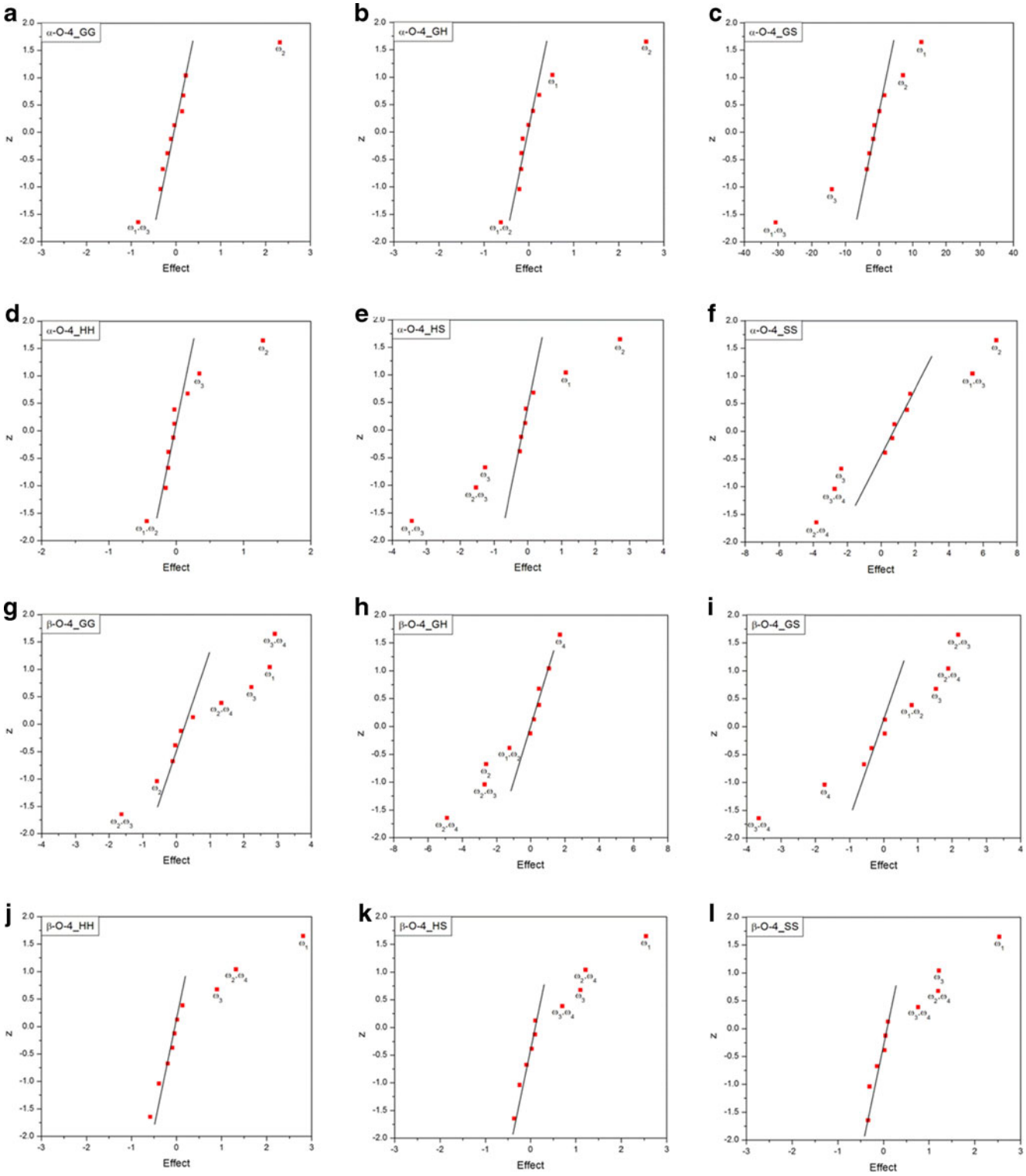

Fig. 5a–l Normal distribution of effects (NDE) for the studied dimers. The points outside the correlation line represent the most relevant dihedrals to be studied. **a** α-O-4_GG; **b** α-O-4_GH; **c** α-O-4_GS; **d** α-O-4_HH; **e** α-O-4_HS; **f** α-O-4_SS; **g** β-O-4_GG; **h** β-O-4_GH; **i** β-O-4_GS; **j** β-O-4_HH; **k** β-O-4_HS; **l** β-O-4_SS

According to (4) we can obtain the values of each dihedral angle that lead to a minimum total energy for each dimer system. It is also important to note that only 3 of the 12 dimers studied presented the initial conformer (S1) as the

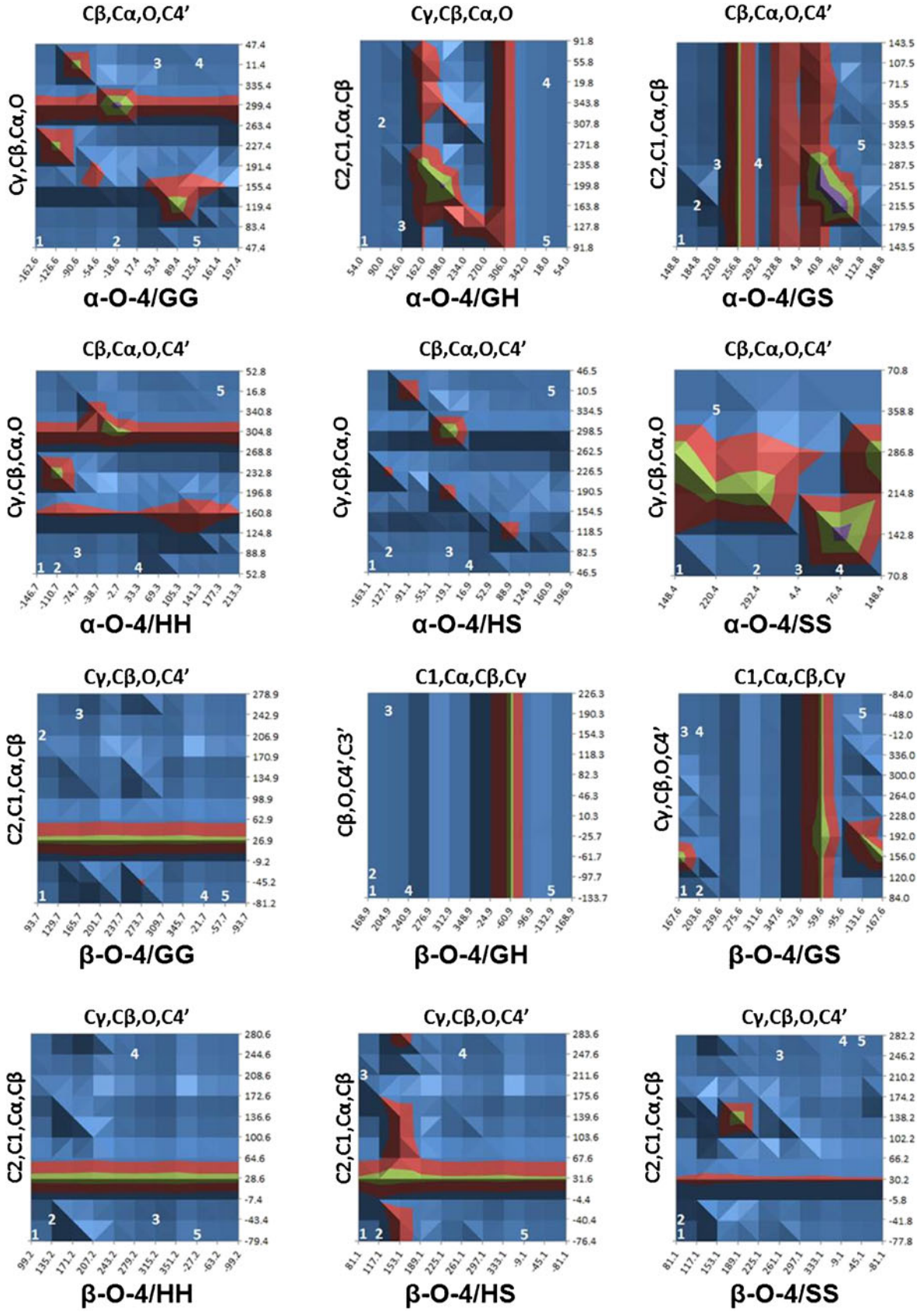

Fig. 6 Potential energy surface (PES) contour maps generated for the lignin α-O-4 and β-O-4 dimers. The labeled points correspond to the five lowest energy minima. *Blue* Low energy values, *bordeaux* medium energy values, *green* high energy values

Table 6 Main dihedral angle values for α-O-4 and β-O-4 dimers

		Dihedral	Dihedral angles values/°								
			S1[a]	S2	S3	S4	S5	L2[b]	L3[b]	L4[b]	BB[c]
α-O-4	GG	ω_2(Cγ,Cβ,Cα,O)	47.4[d]	76.0	47.4	47.4	47.4	50.5	48.3	49.3	47.4
		ω_3(Cβ,Cα,O,C4′)	−163[d]	−140	−163	−163	−163	−164	−162	−163	−163
	GH	ω_1(C2,C1,Cα,Cβ)	91.8	−85.6[d]	117	91.9	91.9	−86.4	−85.2	−92.9	91.8
		ω_2(Cγ,Cβ,Cα,O)	53.9	52.4[d]	167	53.9	53.9	55.7	54.1	57.1	64.4
	GS	ω_1(C2,C1,Cα,Cβ)	144	−40.3[d]	−40.3	−58.2	−40.3	−49.9	−37.9	−53.9	164
		ω_3(Cβ,Cα,O,C4′)	149	151[d]	151	−98.6	151	−170	142	162	149
	HH	ω_2(Cγ,Cβ,Cα,O)	52.8	52.8	73.3[d]	56.3	52.8	58.8	75.2	58.3	52.8
		ω_3(Cβ,Cα,O,C4′)	−147	−147	−157[d]	−154	−147	−154	−158	−158	−147
	HS	ω_2(Cγ,Cβ,Cα,O)	46.5[d]	46.5	77.5	77.5	46.5	48.8	47.7	49.1	78.9
		ω_3(Cβ,Cα,O,C4′)	−163[d]	−163	−58.0	−58.0	−163	−165	−162	−163	−73.1
	SS	ω_2(Cγ,Cβ,Cα,O)	70.8	86.1	78.3	70.8	61.1[d]	−71.1	62.5	−62.1	141
		ω_3(Cβ,Cα,O,C4′)	148	−105.3	−57.5	148	−166[d]	−141	−167	176	−150
β-O-4	GG	ω_1(C2,C1,Cα,Cβ)	−81.1	−81.1	−92.8	−108	−108.2[d]	−83.0	−75.3	−79.3	−81.2
		ω_3(Cγ,Cβ,O,C4′)	93.7	93.7	122	97.4	97.4[d]	88.0	−51.0	87.3	127
	GH	ω_2(C1,Cα,Cβ,Cγ)	169	169	169	−164	−164[d]	178	−162	173	−127
		ω_4(Cβ,O,C4′,C3′)	−134	−134	−134	−123	−123[d]	−123	−147	−152	−82.7
	GS	ω_2(C1,Cα,Cβ,Cγ)	168	168	168	168	−170[d]	178	170	174	−130
		ω_3(Cγ,Cβ,O,C4′)	84.0	84.0	84.0	84.0	128[d]	77.7	58.2	80.5	128
	HH	ω_1(C2,C1,Cα,Cβ)	−79.4[d]	−79.4	−76.9	−76.7	−76.9	−82.5	−80.1	−80.1	−71.2
		ω_3(Cγ,Cβ,O,C4′)	99.2[d]	99.2	−16.9	−17.9	−16.9	91.4	118	108.0	113
	HS	ω_1(C2,C1,Cα,Cβ)	−76.4	−76.4	68.5[d]	−111	−76.4	97.2	179	100	−68.6
		ω_3(Cγ,Cβ,O,C4′)	81.1	81.1	75.9[d]	−115	81.1	75.9	58.1	76.0	112
	SS	ω_1(C2,C1,Cα,Cβ)	−77.8	−77.8	−108	−77.8	−111[d]	−84.3	2.54	−80.0	−73.2
		ω_3(Cγ,Cβ,O,C4′)	81.1	81.1	−102	81.1	31.2[d]	76.5	15.4	77.8	115

[a] Values to the initial optimized structures at HF/6-31G theory level. The geometries S2–S5 were also optimized at HF/6-31G level.

[b] *L2* HF/6-31 + G(2d), *L3* B3LYP/6-31G e *L4* B3LYP/6-31 + G(2d) theory levels. Only the lowest energy structure was considered at higher level of theory

[c] Best dihedral angle values from the adjusted model according to Equation 4

[d] More stable conformers

Table 7 Relative energies (HF/6-31G) for α-O-4 and β-O-4 dimers

Dimers		ΔE_{gas}/kcal mol^{-1}				
		S1[a]	S2	S3	S4	S5
α-O-4	GG	0.00[b]	2.27	3.14×10^{-4}	6.28×10^{-5}	0.00[b]
	GH	0.47	0.00[b]	1.41	0.47	0.47
	GS	0.88	0.00[b]	0.00[b]	1.78	0.00[b]
	HH	2.27	2.27	0.00[b]	1.93	2.27
	HS	0.00[b]	0.00[b]	1.25	1.25	0.00[b]
	SS	1.29	3.39	3.33	1.29	0.00[b]
β-O-4	GG	3.90	3.90	2.52	0.00[b]	0.00[b]
	GH	2.99	2.99	2.99	0.00[b]	0.00[b]
	GS	3.75	3.75	3.75	3.75	0.00[b]
	HH	0.00[b]	0.00[b]	2.17	2.39	2.17
	HS	3.90	3.90	0.00[b]	10.5	3.90
	SS	3.67	3.67	8.79	3.67	0.00[b]

[a] Values corresponding to the initial optimized structures at HF/6-31G theory level. The geometries S2–S5 were also optimized at HF/6-31G level

[b] More stable conformers

most stable, showing the applicability of our protocol to search the conformational space. Some deviations observed are due to "lack of adjustment" of the models and also to the structural peculiarities that may allow structurally equivalent conformers for different angular descriptors (degenerate conformers). Dimers containing equal monomeric units bound by different cross-links have the same number of atoms and, therefore, are position isomers. Figure 7 shows that, in general, the dimers are more stable when linked by α-O-4 than β-O-4 cross-link type. However, the level of theory also plays a role in the stability order as noted for GH and SS dimers, although the energy difference is within 5 kcal mol^{-1}.

Finally, using the conformational data obtained for individual dimers, a larger oligomer was built according to the lignin native composition given in Table 1 and based on an oligomeric structure from the literature [15]. The HF/6-31G optimized structure is shown in Fig. 8. The dihedral angles found were 168° and −135° (ω_2 and ω_4, respectively, for the β-O-4_GH unit), 178° (ω_1 for β-5′_GG unit), 131° (ω_1 for 3–5′_HS unit)

Table 8 Comparison of some dihedral angles between computed lower energy conformers and the crystal structure (Exp.) and theoretical stochastic conformational searching (SCS) for HH and SS β-O-4 models. The values shown are in degrees

Dihedral angle	β-O-4_HH					
	Exp.[a]	S1	S1 (L2)	S1 (L3)	S1 (L4)	SCS[b]
Cα-Cβ-O-C4′	−173	−138	−145	−120	−129	−173
C1-Cα-Cβ-Cγ	178	178	−175	177	−177	–
C1-Cα-Cβ-O	57	59	64	59	64	52
Cβ-O-C4′-C3′	−159	−128	−122	−152	−148	−170
Dihedral angle	β-O-4_SS					
	Exp.[c]	S5	S5 (L2)	S5 (L3)	S5 (L4)	SCS[b]
C6-C1-Cα-Cβ	114	70	96	−177	100	77
C1-Cα-Cβ-O	71	73	65	66	64	−74
C6-C1-Cα-Oα	−123	−166	−142	127	−137	–
Cα-Cβ-O-C4′	151	152	−161	138	−159	−138

[a][33]
[b][5]
[c][34]

and −81.8° and 100° (ω_1 and ω_3, respectively for β-O-4_GG unit) in close agreement to those found for the corresponding dimers. Therefore, a larger structure can be predicted, which is relevant for modeling lignin surface and its chemical processes.

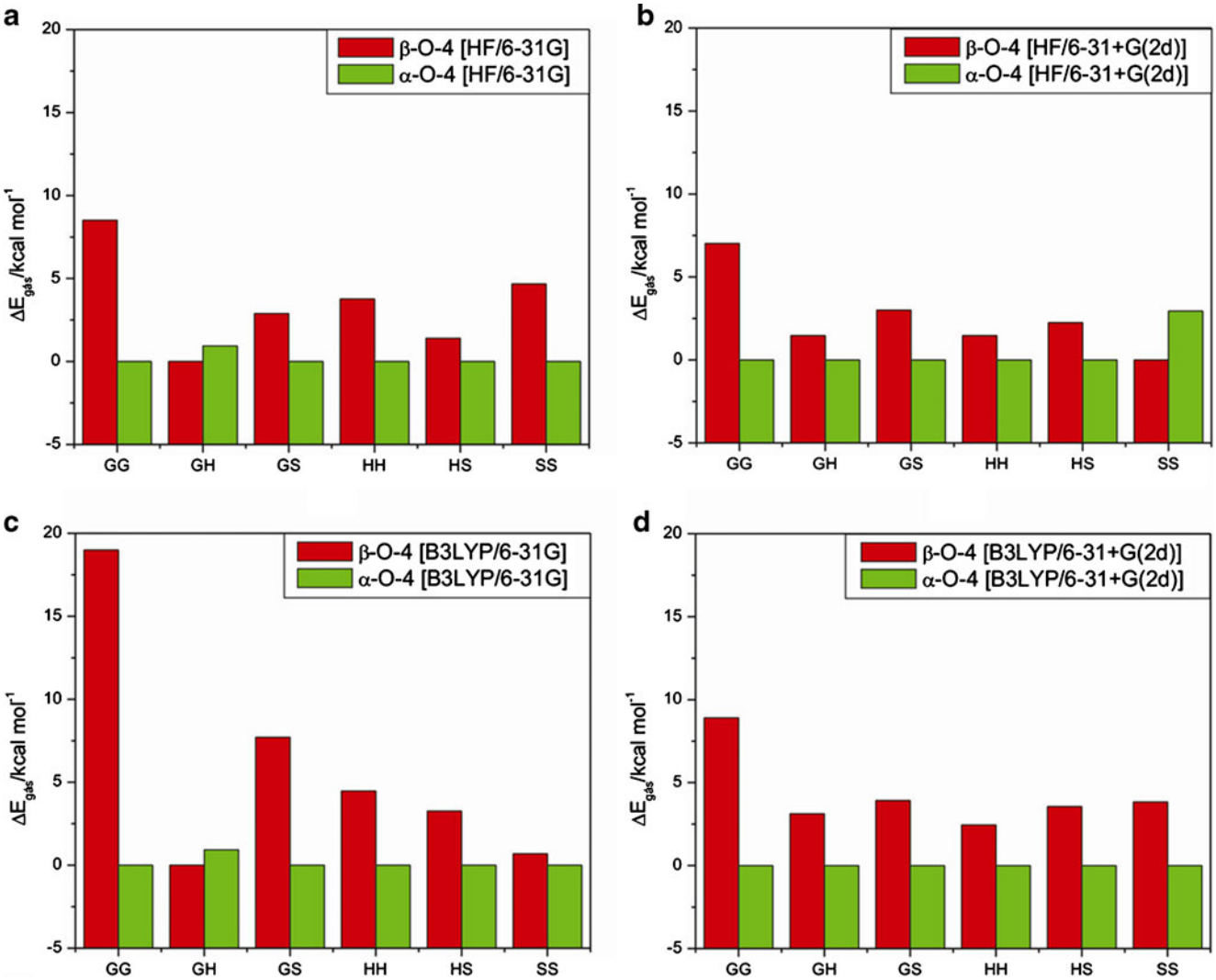

Fig. 7a–d Total gas phase energy variation for α-O-4 and β-O-4 dimers, considering four different levels of theory. The zero value corresponds to the more stable structure for each level of theory. **a** HF/6-31G, **b** HF/6-31 + G(2d), **c** B3LYP/6-31G, **d** B3LYP/6-31 + G(2d)

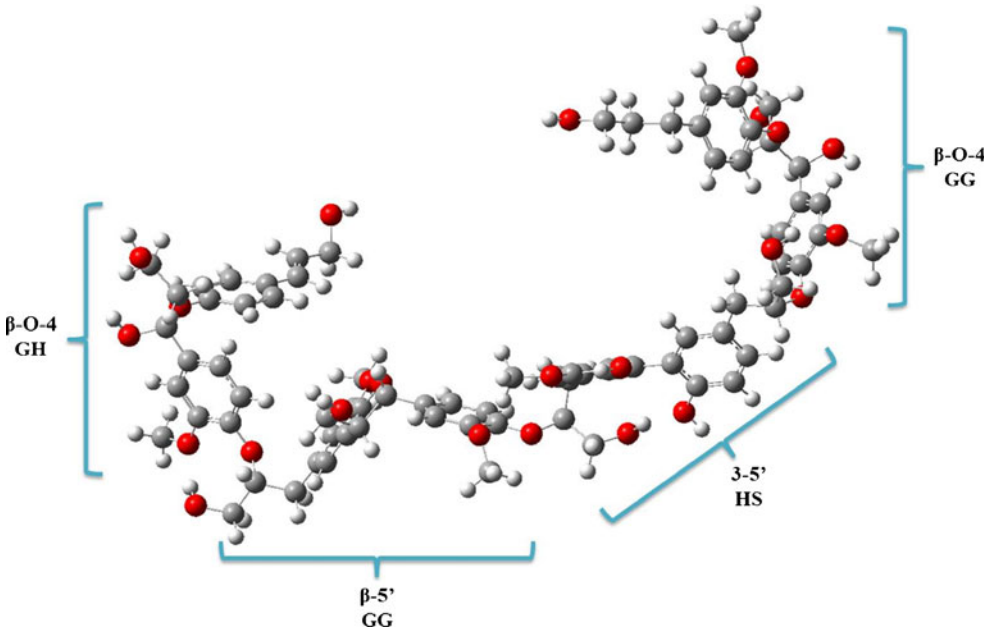

Fig. 8 Optimized structure (HF/6-31G) of a lignin oligomer containing eight units obtained from the small dimers studied here

Conclusions

Conformational analysis of four small lignin models was accomplished using QM methods with the aid of chemometric tools. For the simpler models (3–5′ and β-5′) only one relevant structure was predicted with the inter-monomers dihedral angles found around 126–129° for 3–5′ and 175–179° for β-5′. For these dimers the kind of monomer unit (G, H or S) does not play an important role in the stability, which is driven by cross-link type.

For the larger models (α-O-4 and β-O-4), conformational analysis was carried out using a sequential methodology including QM/BB/QM approaches, where BB analysis was used to screen throughout the four dihedral angles and to select the two most relevant. BB analysis identified the dihedrals $\omega_{2[\alpha\text{-O-4}]}$(Cγ, Cβ, Cα, O) and $\omega_{3[\alpha\text{-O-4}]}$(Cβ, Cα, O, C4′) as the most important for α-O-4 dimers. For β-O-4 structures, the $\omega_{3[\beta\text{-O-4}]}$(Cγ, Cβ, O, C4′) and $\omega_{1[\beta\text{-O-4}]}$(C2, C1, Cα, Cβ) angles were predicted as most important for conformational analysis. These selected dihedrals angles were used to construct the QM PES and the five lowest energy conformers were selected for further analysis. On average, the relative energy is within 5 kcalmol^{-1}, which is in line with the proposal of finding the lowest energy structures. Furthermore, some model compounds studied have shown torsional angles close to crystallographic and theoretical stochastic methodology, which validates the QM/BB/QM conformational method proposed. In this way, the analysis of conformers at higher levels of theory has shown good agreement with crystallographic geometrical parameters, which evidences the importance of the level of theory in the conformational analysis of lignin models. Therefore, from a chemical point of view, the structure found here might be useful to build larger oligomers of lignin in order to explore its potential as a catalyst.

Acknowledgments We thank the Brazilian Agencies CNPq (Conselho Nacional de Desenvolvimento Científico e Tecnológico; National Counsel of Technological and Scientific Development), CAPES (Coordenação de Aperfeiçoamento de Pessoal de Nível Superior; Coordination of Improvement of Higher Education Personel) and FAPEMIG (Fundação de Amparo à Pesquisa do Estado de Minas Gerais) for provision of support to our laboratories. This work is a collaborative research project with members of the Rede Mineira de Química (RQ-MG) supported by FAPEMIG (Project: REDE-113/10). We would also like to thank Prof. Marcone A. L. De Oliveira (UFJF) for helpful comments.

References

1. Phillips M (1934) The chemistry of lignin. Chem Rev 14:103–170
2. Simon JP, Eriksson KEL (1996) The significance of intra-molecular hydrogen bonding in the beta-O-4 linkage of lignin. J Mol Struct 384:1–7
3. Hüttermann A, Mai C, Kharazipour A (2001) Modification of lignin for the production of new compounded materials. Appl Microbiol Biotechnol 55:387–384
4. Ikeda T, Holtman K, Kadla JF, Chang HM, Jameel H (2002) Studies on the effect of ball milling on lignin structure using a modified DFRC method. J Agric Food Chem 50:129–135
5. Besombes S, Robert D, Utille JP, Taravel FR, Mazeau K (2003) Molecular modeling of syringyl and p-hydroxyphenyl β-O-4 dimers. Comparative study of the computed and experimental conformational properties of lignin β-O-4 model compounds. J Agric Food Chem 51:34–42
6. Boerjan W, Ralph J, Baucher M (2003) Lignin biosynthesis. Annu Rev Plant Biol 54:519–546
7. Agache C, Popa VI (2006) Ab initio studies on the molecular conformation of lignin model compounds I. Conformational

preferences of the phenolic hydroxyl and methoxy groups in guaiacol. Monatsh Chem 137:55–68
8. Notley SM, Norgren M (2006) Measurement of interaction forces between lignin and cellulose as a function of aqueous electrolyte solution conditions. Langmuir 22:11199–11204
9. Suhas, Carrott PJM, Ribeiro Carrott MML (2007) Lignin—from natural adsorbent to activated carbon: a review. Bioresour Technol 98:2301–2312
10. Larsen KL, Barsberg S (2010) Theoretical and Raman spectroscopic studies of phenolic lignin model monomers. J Phys Chem B 114:8009–8021
11. Sazanov YN, Gribanov AV (2010) Thermochemistry of lignin. Russ J Appl Chem 83:175–194
12. Zakzeski J, Bruijnincx PCA, Jongerius AL, Weckhuysen BM (2010) The catalytic valorization of lignin for the production of renewable chemicals. Chem Rev 110:3552–3599
13. Karmanov AP, Belyaev VY, Kocheva LS (2011) A study of the structure of lignin macromolecules. Russ J Bioorg Chem 37:842–848
14. Kim S, Chmely SC, Nimlos MR, Bomble YJ, Foust TD, Paton RS, Beckham GT (2011) Computational study of bond dissociation enthalpies for a large range of native and modified lignins. J Phys Chem Lett 2:2846–2852
15. Sjöström E (1981) Wood chemistry—fundamentals and applications. Academic, New York
16. Dos Santos HF (2001) Análise Conformacional de modelos de lignina. Quím Nova 24:480–490
17. Mazeau K, Rinaudo M (2004) The prediction of the characteristics of some polysaccharides from molecular modeling. Comparison with effective behavior. Food Hydrocoll 18:885–898
18. Sangha AK, Petridis L, Smith JC, Ziebell A, Parks JM (2012) Molecular simulation as a tool for studying lignin. Environ Prog Sustain Energy 31:47–54
19. Petridis L, Schulz R, Smith JC (2011) Simulation analysis of the temperature dependence of lignin structure and dynamics. J Am Chem Soc 133:20277–20287
20. Zhang L, LeBoeuf EJ (2009) A molecular dynamics study of natural organic matter: 1. Lignin, kerogen and soot. Org Geochem 40:1132–1142
21. Petridis L, Smith JC (2008) A molecular mechanics force field for lignin. J Comput Chem 30:457–467
22. Besombes S, Utille JP, Mazeau K, Robert D, Taravel FR (2004) Conformational study of a guaiacyl beta-O-4 lignin model compound by NMR. Examination of intramolecular hydrogen bonding interactions and conformational flexibility in solution. Magn Reson Chem 42:337–347
23. Besombes S, Mazeau K (2004) Molecular dynamics simulations of a guaiacyl beta-O-4 lignin model compound: examination of intramolecular hydrogen bonding and conformational flexibility. Biopolym 73:301–315
24. Vu T, Chaffee A, Yarovsky I (2002) Investigation of lignin-water interactions by molecular simulation. Mol Simul 28:981–991
25. Besombes S, Robert D, Utille JP, Taravel FR, Mazeau K (2003) Molecular modeling of lignin beta-O-4 model compounds. Comparative study of the computed and experimental conformational properties for a guaiacyl beta-O-4 dimer. Holzforschung 57:266–274
26. Li XY, Eriksson LA (2005) Molecular dynamics study of lignin constituents in water. Holzforschung 59:253–262
27. Almeida EWC, Anconi CPA, Novato WTG, De Oliveira MAL, De Almeida WB, Dos Santos HF (2011) Box-Behnken design for studying inclusion complexes of triglycerides and α-cyclodextrin: application to the heating protocol in molecular-dynamics simulations. J Incl Phenom Macrocycl Chem 71:103–111
28. Frisch MJ, Trucks GW, Schlegel HB, Scuseria GE, Robb MA, Cheeseman JR, Montgomery JA, Vreven T, Kudin KN, Burant JC, Millam JM, Iyengar SS, Tomasi J, Barone V, Mennucci B, Cossi M, Scalmani G, Rega N, Petersson GA, Nakatsuji H, Hada M, Ehara M, Toyota K, Fukuda R, Hasegawa J, Ishida M, Nakajima T, Honda Y, Kitao O, Nakai H, Klene M, Li X, Knox JE, Hratchian HP, Cross JB, Adamo C, Jaramillo J, Gomperts R, Stratmann RE, Yazyev O, Austin AJ, Cammi R, Pomelli C, Ochterski JW, Ayala PY, Morokuma K, Voth GA, Salvador P, Dannenberg JJ, Zakrzewski VG, Dapprich S, Daniels AD, Strain MC, Farkas O, Malick DK, Rabuck AD, Raghavachari K, Foresman JB, Ortiz JV, Cui Q, Baboul AG, Clifford S, Cioslowski J, Stefanov BB, Liu G, Liashenko A, Piskorz P, Komaromi I, Martin RL, Fox DJ, Keith T, Al-Laham MA, Peng CY, Nanayakkara A, Challacombe M, Gill PMW, Johnson B, Chen W, Wong MW, Gonzalez C, Pople JA (2004) Gaussian 03, revision D.01. Gaussian, Wallingford
29. Ferreira SLC, Bruns RE, Ferreira HS, Matos GD, David JM, Brand GC, Silva EGP, Reis PS, Souza AS, Santos WNL (2007) Box-Behnken design: an alternative for the optimization of analytical methods. Anal Chim Acta 597:179–186
30. Roblin J, Duran H, Duran E, Gorrichon L (2000) X-ray structure of a trimeric 5,5′-Biaryl/erythro-β-O-4-ether Lignin model: evidence for through-space weak interactions. Chem Eur J 6:1229–1235
31. Johansson MP, Olsen J (2008) Torsional barriers and equilibrium angle of biphenyl. J Chem Theor Comput 4:1460–1471
32. Stomberg R, Lundquist K (1987) The crystal structure of trans-2,3-Dihydro-2-(4-hydroxy-3-methoxyphenyl)-3-hydroxymethyl-7-methoxybenzofuran. Acta Chem Scand B41:304–309
33. Johansson A, Lundquist K, Stomberg R (1992) Stereochemistry of arylglycerol beta-Aryl Ethers. Crystal structure of erythro-3-hydroxy-3-(4-methoxyphenyl)-2-phenoxypropanoic Acid. Acta Chem Scand 46:901–905
34. Stomberg R, Lundquist K (1989) On the stereochemistry of lignin model compounds of the arylglycerol-beta-aryl ether type: Crystal structure of erythro-1-(4-hydroxy-3,5-dimethoxyphenyl)-2-(4-hydroxymethil-2,6-dimethoxyphenoxy)-1,3-propanediol, $C_{20}H_{26}O_9$. J Crystallogr Spectrosc Res 19:331–339